

# Alternating projection-based phase optimization for arbitrary glare suppression through multimode fiber

Shengfu Cheng<sup>a,b,1</sup>, Tianting Zhong<sup>a,b,1</sup>, Chi Man Woo<sup>a,b</sup>, Puxiang Lai<sup>a,b,c,\*</sup>

<sup>a</sup> Department of Biomedical Engineering, The Hong Kong Polytechnic University, Hong Kong Special Administrative Region

<sup>b</sup> The Hong Kong Polytechnic University Shenzhen Research Institute, Shenzhen, China

<sup>c</sup> Photonics Research Institute, The Hong Kong Polytechnic University, Hong Kong Special Administrative Region

## ARTICLE INFO

### Keywords:

Glare suppression  
Wavefront shaping  
Alternating projection algorithm

## ABSTRACT

Wavefront shaping for glare suppression helps to reduce the speckle background through scattering media and enables imaging, sensing, and some speckle-related advanced applications through customizing the speckle light field. For glare suppression in a target region, current methods are either slow or not sufficiently generic. Here, an alternating projection method that fully exploits the transmission matrix of the scattering medium is proposed for fast and arbitrary glare suppression. Parallely, multiple phase masks corresponding to different target regions can be computationally optimized without iterative hardware feedback. Numerical simulation shows that under phase-only modulation, a suppression factor of  $\sim 10^{-3}$  can be realized for a large target region with only 30 iterations. With the use of a graphics processing unit and a digital micromirror device, fast and effective glare suppression for target regions of various shapes and sizes was demonstrated at the distal end of a multimode fiber. This technique could be promising for applications like multimode fiber-based speckle optical tweezer or endoscopy with speckle illumination inside complex environments.

## 1. Introduction

Glare suppression was originally proposed for some imaging or sensing scenarios under the reflection geometry [1,2]. For example, during the detection of a weak object hidden behind a scattering medium, the glare from unwanted backscattered light by the medium may seriously degrade the signal-to-noise ratio (SNR). Such a phenomenon could occur in LiDAR detection through atmosphere or ocean, deep-tissue optical imaging, or even broader electromagnetic scenarios such as microwave-based detection. In these cases, the ability to suppress glare enables imaging or sensing of weak objects in the absence of a strong background. In principle, glare suppression is feasible based on the time-of-flight differences between the target signal and the backscattered light, although the approaches are usually costly with limited temporal resolution [2]. Coherence gating [3] can also reject glare by only detecting the target signal that is coherent to the reference light. Not long ago, a coherence gated negation technique was reported, which actively “gates out” the glare component by utilizing a low-coherence source [2]. Nevertheless, both methods are technically demanding.

Apart from these studies in reflection mode, suppressing the scattered light intensity in a transmission geometry is also valuable for imaging and sensing. Furthermore, custom-tailoring a speckle field with

blank window could be attractive for applications that employ speckle fields for optical tweezer [4] or structured illumination microscopy [5]. Recent developments of glare suppression through scattering media are primarily facilitated by wavefront shaping (WFS), a powerful tool to control the propagation of diffused light [6–10]. By constructing a transmission matrix (TM) [11] that relates the input and output fields of the optical medium, one can deterministically shape the output light field by applying appropriate modulation to the input wavefront. WFS can also be iterative [12–17] when the TM is inaccessible, which, however, lacks a versatile ability for light manipulation. With the knowledge of TM, any desired optical field can be theoretically realized despite light scattering. WFS has been widely applied to focus diffused light, which enables high-resolution point-scanning imaging [18] or localized optical energy delivery-related biomedical applications [19,20] at depths. Besides that, WFS also offers potentials for the suppression of scattered glare through scattering media [1,21,22].

Recent efforts started with the iterative methods. Daniel et al. first adopted a genetic algorithm (GA) to reduce the integrated intensity of a selected region containing  $\sim 36$  speckle grains to  $\sim 17\%$  of its initial value after 1000 iterations [1]. Later, a Hadamard encoding algorithm was explored that showed improved performance than GA in reducing the intensities of both single and multiple speckle grains [21]. These methods

\* Corresponding author at: Department of Biomedical Engineering, The Hong Kong Polytechnic University, Hong Kong Special Administrative Region.  
E-mail address: [puxiang.lai@polyu.edu.hk](mailto:puxiang.lai@polyu.edu.hk) (P. Lai).

<sup>1</sup> These authors contributed equally to this work.

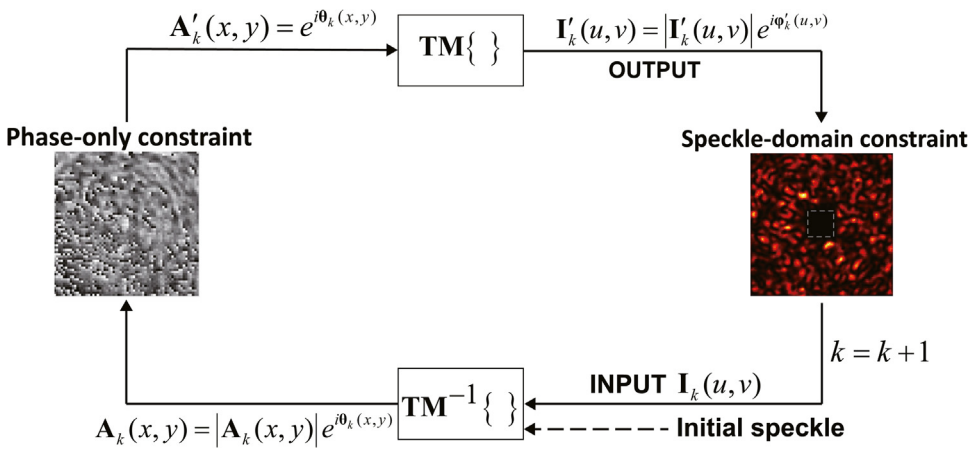


**Fig. 1.** Schematic of the proposed alternating projection method to obtain the optimum phase mask for glare suppression at a target region within the speckle field.

could be time-consuming because of their nature of feedback-based iterative optimization and the use of a spatial light modulator (SLM) with slow refresh rate (typically 60 Hz). More recently, an aperture-target TM model was proposed using the low-transmittance eigenchannel as the input wavefront to achieve minimal speckle intensity in the target area [22]. Although the optimization results were superior, the method relied on an amplitude-phase modulation and might not be generic enough, as a new aperture-target TM for decomposition was required for each target region.

In this letter, we show that an alternating projection-based phase optimization can be used for fast and arbitrary glare suppression through scattering media. With the knowledge of TM, multiple phase masks that correspond to different target regions can be optimized in parallel, requiring only a few tens of iterations in practice. It is stressed that the method is purely computational that involves no hardware feedback, and the operation is further accelerated by implementation with a graphics processing unit (GPU). Numerical simulation reveals that a suppression factor of  $\sim 10^{-3}$  is achieved even for a large target region that contains over a hundred speckles, under phase-only modulation. Experimentally, fast and effective glare suppression has been realized in target regions of various shapes and sizes at the distal end of a multimode fiber (MMF) by using a digital micromirror device (DMD) as the SLM.

## 2. Methods

We get inspiration from the problem of phase retrieval solved by using the Gerchberg–Saxton (GS) algorithm [23,24]. The basic idea of GS algorithm is to retrieve the phase of an object from the intensity measurement of its diffraction pattern (*i.e.*, the Fourier transform of the object) via alternating projection between the object plane and the Fourier plane. Such an iterative Fourier transform algorithm was first developed in 1970s, and has found many variants that see applications in electron microscopy, crystallography, synthesis of computer hologram etc. [25]. Here, we propose to optimize the phase mask for the suppression of speckle light intensity at a target region by alternating projection between the phase and speckle planes of a scattering medium, utilizing TM as the propagation operator.

Fig. 1 depicts the process of alternating projection-based phase optimization used for glare suppression. Suppose the scattering medium is a linear system through which light propagates between the phase and speckle fields. The algorithm starts with an initial speckle pattern produced under zero-phase modulation. At the  $k$ th iteration, the inverse TM transforms the estimated speckle field  $I_k(u, v)$  into the phase field  $A_k(x, y)$ ,

$$A_k(x, y) = |A_k(x, y)|e^{i\theta_k(x, y)} = TM^{-1}\{I_k(u, v)\}, \quad (1)$$

where  $\theta_k(x, y)$  is the phase of the resultant input wavefront. Here, the Tikhonov inversion [26] is adopted, which helps mitigate the measurement noise of TM and allows more accurate modeling of the back-propagation of light. The phase-only constraint sets the amplitudes of the input wavefront all to be one, such that

$$A'_k(x, y) = e^{i\theta_k(x, y)}. \quad (2)$$

The new phase field  $A'_k(x, y)$  then propagates towards the speckle domain  $I'_k(u, v)$ ,

$$I'_k(u, v) = |I'_k(u, v)|e^{i\phi'_k(u, v)} = TM\{A'_k(x, y)\}, \quad (3)$$

where  $\phi'_k(u, v)$  is the phase of the resultant speckle field. Similarly, a constraint is applied on the speckle domain to force an intensity reduction in the target region. The updated speckle field  $I_{k+1}(u, v)$  continues the above processes iteratively, with the goal of estimating a solution that conforms to both constraints simultaneously.

One natural choice of the speckle-domain constraint is setting the values of the points within the target region (represented by  $T$ ) to be 0, given by

$$I_{k+1}(u, v) = \begin{cases} 0, & (u, v) \in T \\ I'_k(u, v), & (u, v) \notin T \end{cases} \quad (4)$$

This constraint is consistent with the error-reduction (ER) algorithm [23,27], a variant of GS algorithm, which is based on the idea that in a phase retrieval problem, the object cannot be negative or exceed the known diameter. However, it has been observed that the ER algorithm tends to reach a plateau after the first few iterations and the convergence later on is relatively slow. A modification is the hybrid input-output (HIO) algorithm [24,27]. The alternating projection streaming can be regarded as an input-output system, with the produced speckle field as the output and the updated one as the system input for the next iteration, as illustrated in Fig. 1. For the pixels outside of the target region, one does not require a change of the output. But for those within the target region, HIO applies negative feedback upon the previous input  $I_k(u, v)$  using the iteration output  $I'_k(u, v)$  to generate the next input, such as

$$I_{k+1}(u, v) = \begin{cases} I_k(u, v) - \gamma \cdot I'_k(u, v), & (u, v) \in T \\ I'_k(u, v), & (u, v) \notin T \end{cases} \quad (5)$$

where  $\gamma$  is the feedback coefficient. The output at the target region is driven to a value of zero due to a decrease of the input. HIO is supposed to have faster convergence as it could avoid a stagnation problem occurred in the ER algorithm. The convergence property of the proposed alternating projection method used for glare suppression is shown in appendix I. In the next session, alternating projection-based phase optimization using speckle-domain constraints of both ER and HIO will be conducted to test their performances in reducing intensity in the target regions through simulations and experiments.

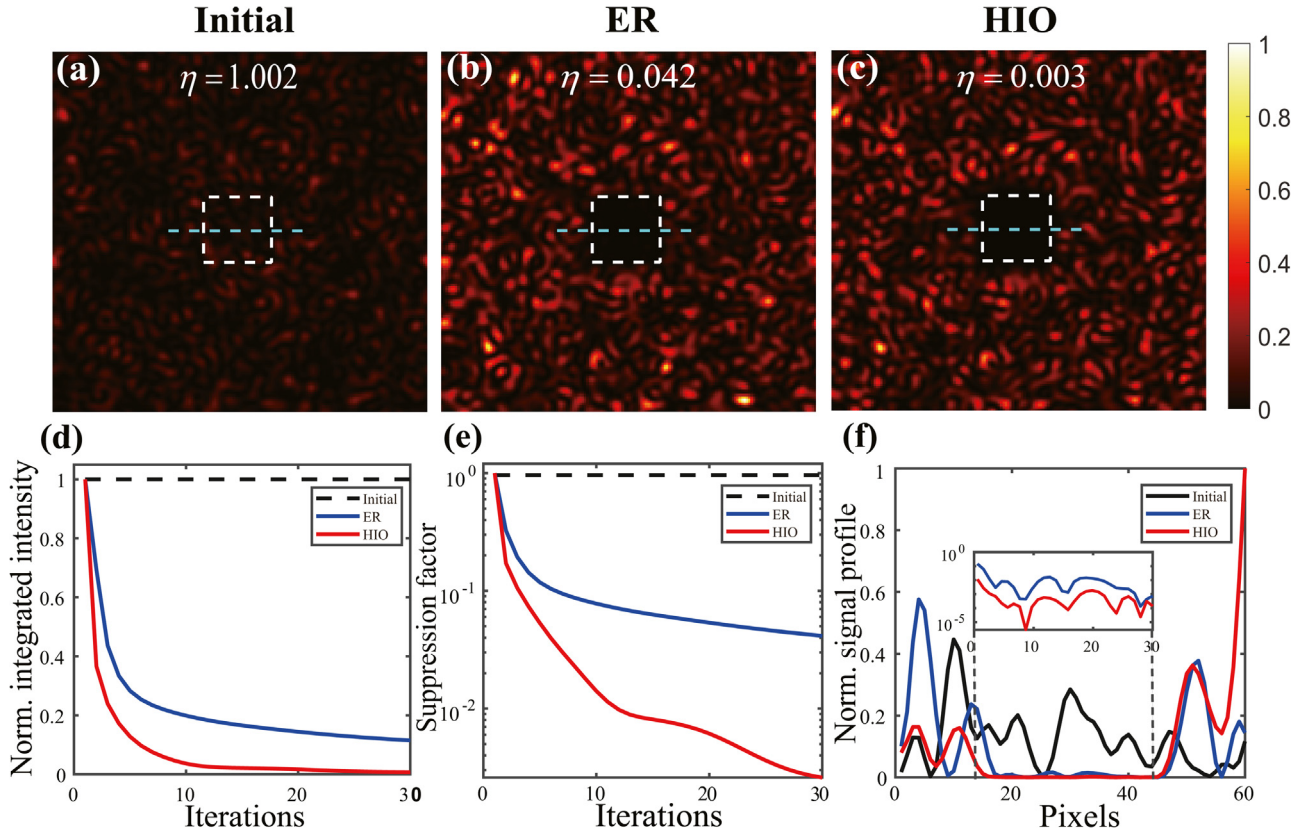


**Fig. 2.** Simulated results of glare suppression for a square region with a side length of 30 pixels in the speckle field, using the proposed alternating projection method with different speckle-domain constraints. (a) Initial speckle pattern with zero phase modulation. (b) Optimized with ER constraint; (c) Optimized with HIO constraint. (d) Progression curves of the normalized integrated intensity in the target regions for ER and HIO. (e) Progression curves of suppression factor as a function of iteration number. (f) Normalized signal profiles along the cyan dashed line segments in (a–c), in which the inset magnifies the ER and HIO's profiles corresponding to the target region.

### 3. Numerical simulation

The capability of our alternating projection method for glare suppression was first investigated via numerical simulation. The number of modulation units was set to be  $64 \times 64$ , with an output light field of  $160 \times 160$  pixels. The TM was simulated by modeling the speckle field using random phase with zero padding in the Fourier space, in which the size of a speckle grain was 4, a number comparable to the real observation. As a proof-of-principle study, alternating projection optimized with both types of speckle-domain constraints, ER and HIO, was explored for the comparison of suppression performance. Herein, the feedback coefficient  $\gamma$  of HIO was empirically set to be 0.8 to ensure quick and stable convergence. To evaluate the suppression effect, a suppression factor  $\eta$  is defined as the ratio of the mean light intensity of the target region over that outside the target region, such that

$$\eta = \mu(|\mathbf{I}_i|)_{i \in T} / \mu(|\mathbf{I}_i|)_{i \notin T}, \quad (6)$$

Where  $\mu(\cdot)$  denotes the mean operation,  $T$  represents the target region, and  $\mathbf{I}_i$  is the complex amplitude at position index  $i$  in the speckle field.

Fig. 2 shows the simulated glare suppression results using speckle-domain constraints of ER and HIO, respectively, with an iteration number of 30 for achieving an acceptable suppression result with a short time consumption. The region of interest (ROI) is a square of  $30 \times 30$  pixels in the middle of the speckle field, marked with white dashed boxes in Fig. 2(a–c). The initial speckle pattern (Fig. 2a) has an almost uniform intensity distribution across the whole field of view (FOV), with  $\eta \approx 1$ . In comparison, the light intensities within the ROI are adequately suppressed for those optimized with both ER (Fig. 2b,  $\eta = 0.042$ ) and HIO (Fig. 2c,  $\eta = 0.003$ ). Quantitatively, the normalized integrated speckle in-

tensity of the ROI declines progressively during 30 iterations for both ER and HIO, while only HIO could converge closely to zero, as seen in Fig. 2d. The progression curves of suppression factor as a function of iteration number are shown in Fig. 2e, which also reveals that HIO declines faster and achieves superior suppression effect than ER does. More specifically, the normalized signal profiles across the ROI, denoted by the cyan dashed line segments in Figs. 2a–c, are also compared in Fig. 2f. It can be seen that the signal intensities within the ROI (15th ~ 45th pixels) are reduced to almost zero for ER and HIO. A closer look (the inset in Fig. 2f) shows that HIO can suppress the signal to a lower level. The above simulation results suggest that our method is effective in glare suppression and fast in convergence, and the performance of HIO is superior to that of ER. Note that the non-target regions in Fig. 2b and c seem to be brighter than that before suppression, which should not affect the conclusion as we only concern the integrated intensity in the target region and the suppression effect.

Numerical comparisons were also made between the alternating projection method and the state-of-the-art GA to test their performances of glare suppression in square regions of various sizes (denoted by the side length  $L$ ). The controlled phase mask was at the dimension of  $64 \times 64$  for both methods. The parameters of GA were set as follows: the initial and final mutation rates were 0.01 and 0.001, respectively; the decay factor was 250; the population size was 30; and the iteration number was 1200. For our method, although the iteration number required for convergence may be large and vary with different ROI sizes, an iteration number of only 30 was adopted in practice for both ER and HIO. This allows it to achieve a suppression factor ( $\sim 10^{-2}$ ) comparable to that of GA with 1200 iterations by consuming much less running time. Specifically, it took an average of 12.03 s for GA, while only 0.54 s

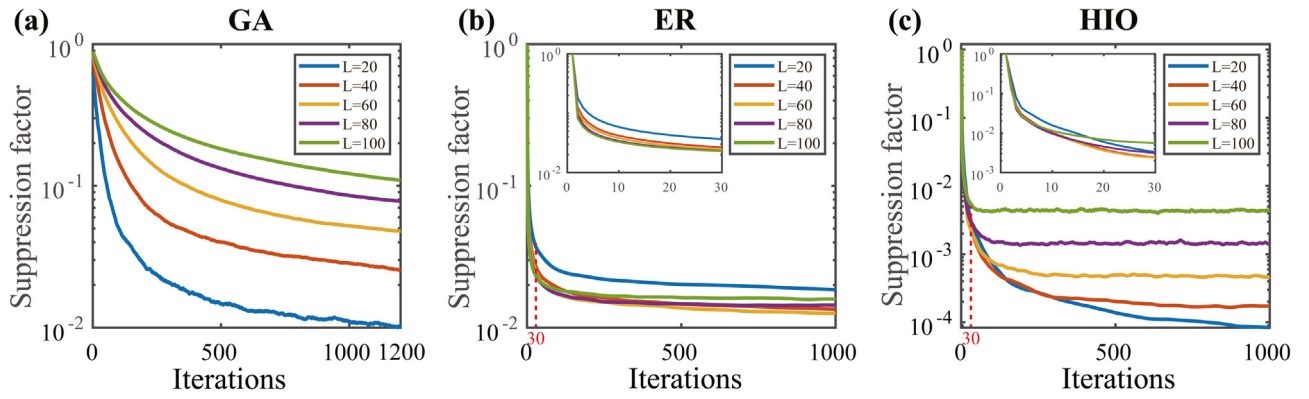


**Fig. 3.** Simulated progression curves of suppression factor as a function of iteration number in the square ROIs of different side lengths, when using (a) GA, and alternating projection method with speckle-domain constraints of (b) ER and (c) HIO, respectively. Note that the subplots inside (b) and (c) show the zoomed-in results within the first 30 iterations.

for ER and 0.46 s for HIO, when running on GPU at the environment of MATLAB 2022a by using a PC with an Intel Xeon CPU (3.50 GHz), NVIDIA 3070 GPU and 64 GB RAM. To reduce randomness, for each side length  $L$ , the result of each algorithm was averaged over 30 repetitions, where a new TM was simulated each time. Fig. 3 shows the simulated progression curves for GA and our method optimized with ER and HIO, respectively. Cases of ER and HIO are both plotted with 1000 iterations to show the theoretical performances that can be achieved. From Fig. 3a, it can be seen that the suppression effect of GA enhances ( $\eta$  declined from  $\sim 0.1$  to  $\sim 0.01$ ) as the side length of the ROI decreases from 100 to 20. This is reasonable as the number of phase control segments remains unchanged. For the alternating projection method with ER constraint (Fig. 3b), it converges prematurely after several hundred iterations for different ROIs, with relatively poor performance ( $\eta > 0.01$ ) in intensity suppression. Note that there is no rule between the sizes of ROIs to be suppressed and the achieved suppression factors in this case, and no significant difference of suppression performance in different ROIs. In contrast, when using the HIO constraint (Fig. 3c), the suppression ability of our method can be fully exerted, achieving hierarchical suppression results for ROIs of different sizes that are all considerably superior to those of GA and ER. Note that in practice, the optimization only runs for 30 iterations after which the achieved suppression factor is almost at a level of  $10^{-3}$  theoretically, with no obvious differences among different ROIs. Interestingly, there is a turning point for the cases of  $L = 20$  and  $L = 100$  (the inset in Fig. 3c), suggesting that the suppression factor of  $100 \times 100$  ROI initially declines faster while that of  $20 \times 20$  ROI converges to a lower level eventually. The reason might be that the intensity suppression within the  $100 \times 100$  region is more stable on average and converges more soothingly in the initial phase, especially when there is a strong modulation capability. Further analysis on the performance of our method in intensity suppression for ROIs of various sizes and with different numbers of modulation units can be found in appendix II.

#### 4. Experimental results

The experimental setup for TM measurement and glare suppression through a multimode fiber is illustrated in Fig. 4. The light output from a 532 nm continuous-wave laser (EXLSR-532-300-CDRH, Spectra Physics, USA) was first divided into two beams by a polarizing beam splitter (PBS) after passing through a half-wave ( $\lambda/2$ ) plate. One beam was used as the reference beam, which was expanded by a 4f lens system (L5 and L6), with its polarization state being adjusted by a  $\lambda/2$  plate. The other beam was expanded by a 40 $\times$  objective lens (Obj1) and collimated by a convex lens (L1) subsequently. After turning to be circularly polarized light by a quarter-wave ( $\lambda/4$ ) plate, the beam was reflected by a DMD (DLP7000, Texas Instruments Inc, USA) and relayed into another 4f system (L2, iris, and L3). After spectral filtering, the beam encoded

with the desired phase distribution [28,29] was coupled into a MMF (0.22 numerical aperture, 105  $\mu\text{m}$  core, SUH105, Xinrui, China) that was used as the scattering medium in this study. The beam after propagating through the MMF was magnified by a 40 $\times$  objective (Obj2) and collimated by a tube lens L4. A  $\lambda/4$  plate was used to recover the linearly polarized components of the disordered beam. The speckle and the reference light paths were combined by a non-polarized beam splitter (NPBS) for interference before being captured by a CMOS camera (BFS-U3-04S2M, FLIR, USA). Note that the CMOS camera was triggered by the DMD and would capture an image once the DMD displays a pattern. With the recorded interferograms, spatial filtering-based digital holography method [30] was employed for retrieving the complex TM of the MMF.

In experiment, the sizes of the controlled phase masks and the captured speckle patterns were the same as those in simulation. Besides that, GA and alternating projection method optimized with ER and HIO were all conducted for performance comparison, with the parameter settings unchanged, too. The TM of the MMF was first calibrated and then used to optimize the phase mask via different algorithms that were implemented by GPU. It should be noted that no hardware feedback was involved and the phase optimizations for both GA and the alternating projection method were based on the same TM for fair comparison. One particular advantage of our method is that multiple phase masks that correspond to different ROIs can be optimized in parallel. For example, it only took  $\sim 2.3$  s to optimize 120 frames of phase masks simultaneously, equivalent to  $\sim 22.5$  ms/frame. This was much faster than the sequential optimization, which required  $\sim 0.5$  s to optimize one single phase mask. The optimized phase masks were encoded into binary Lee holograms [29] and uploaded onto the DMD for phase-only modulation to the incident light. The glare suppression results at the distal end of the MMF were captured by the CMOS camera synchronously. A maximum frame rate of  $\sim 50$  fps was achieved for real-time glare suppression through MMF.

Fig. 5 shows the normalized speckle images that were obtained under zero phase modulation or optimized GA and our method (with ER and HIO constraint), for ROIs of different sizes. The autocorrelation of the initial speckle patterns revealed that the size of a speckle grain was  $4 \times 4$  pixels on average in our experiment. The first row of Fig. 5 corresponds to a square ROI with  $40 \times 40$  pixels, which contains  $\sim 100$  speckles. Compared to the simulated results in Fig. 3, where GA achieves  $\eta = 0.025$  after 1200 iterations and ER achieves  $\eta = 0.028$  after 30 iterations, the suppression factors realized in experiment are almost one order-of-magnitude worse in both cases. For HIO, the suppression effect ( $\eta = 0.15$ ) is undoubtedly better than GA and ER, although still almost two order-of-magnitude worse than the simulated one ( $\eta = 0.0024$ ). The second row of Fig. 5 represents the results for a ROI of  $100 \times 100$  pixels where  $\sim 625$  speckles are contained. Compared to the cases in the first row, the performance of glare suppression is slightly worse for GA

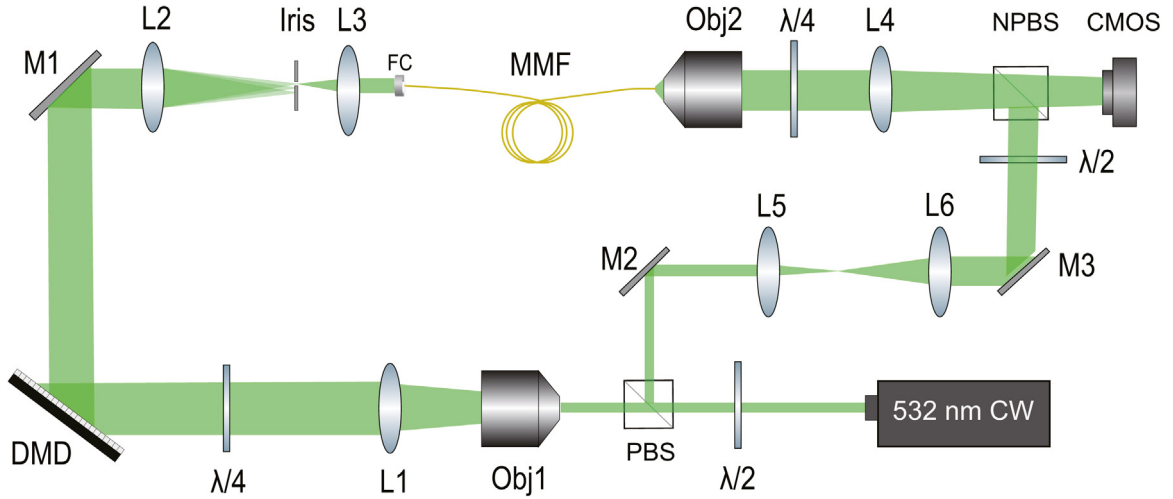


Fig. 4. Experimental setup for glare suppression through a MMF. The complex TM of the MMF is measured via off-axis holography, and a DMD is used for phase-only modulation. CMOS, complementary metal-oxide-semiconductor camera; DMD, digital mirror device; FC, fiber collimator; L, lens; M, mirror; MMF, multimode fiber; NPBS, non-polarizing beam splitter; Obj, objective; PBS, polarizing beam splitter;  $\lambda/2$ , half-wave plate;  $\lambda/4$ , quarter-wave plate.

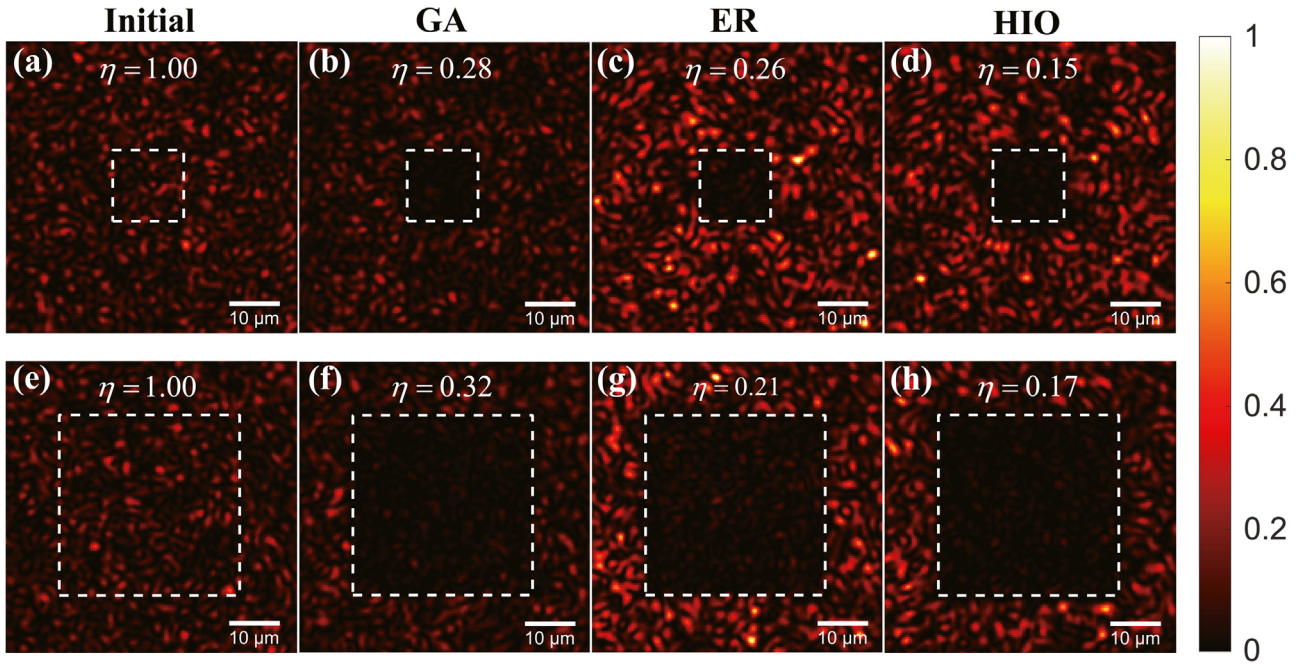


Fig. 5. Normalized speckle patterns showing glare suppression in ROIs of various sizes at the distal end of the MMF, using different algorithms for comparison. The first row and second row correspond to square regions of  $40 \times 40$  pixels and  $100 \times 100$  pixels, respectively, with (a, e) for the initial speckle pattern under zero phase modulation, (b, f) for those optimized with GA after 1200 iterations, (c, g) for those optimized with ER after 30 iterations, and (d, h) for those optimized with HIO after 30 iterations. The scale bar shown in (a–h) is  $10 \mu\text{m}$ .

( $\eta = 0.32$ ) and HIO ( $\eta = 0.17$ ), but slightly better for ER ( $\eta = 0.21$ ). In summary, the obtained experimental results agree reasonably with the simulated ones as shown in Fig. 3. Although the case of ER might seem to be counterintuitive that the  $100 \times 100$  region yields a slightly better suppression factor than the  $40 \times 40$  region, it is understandable as ER is prone to suffer from premature convergence. Moreover, the optimization has not yet fully converged at the 30-th iteration. Further discussion can be found in appendix II. Apart from the results shown in Fig. 5, fast and effective glare suppression in arbitrary regions of different shapes and sizes at the distal end of MMF has been demonstrated experimentally (Media1) using HIO constraint. It is believed that the technique could be promising for speckle optical tweezer with flexibility [4] or super-resolution endoscopic imaging [5] inside deep tissues through the MMF, where the customized speckle fields would be utilized.

## 5. Discussions and conclusions

We present an alternating projection-based phase optimization method by exploiting the TM for glare suppression at arbitrary regions through scattering media such as MMF. In practice, only dozens of iterations are required to find an appropriate phase mask that achieves a theoretical suppression factor of  $\sim 10^{-3}$ . The optimization process can be quick and in parallel (e.g., 2.27 s for 120 frames of  $64 \times 64$  phase masks). Although the TM method in wavefront shaping has been used to focus light into single spot or a pattern [31], currently there lacks a generic way to obtain the desired phase mask for arbitrary glare suppression with the use of a single TM. A recent study relies on the single value composition of an aperture-target TM, which only applies to a specific target region [22]. Apart from the capability of arbitrary intensity

suppression, this alternating projection method can also be extended to produce any desired target pattern through scattering media. By modifying the speckle-domain constraint, generating a focal pattern with high fidelity through scattering media [20] is also feasible. However, the study also has some limitations. The first is the requirement of measuring a complex TM, which could sometimes be demanding due to the additional system complexity for a reference beam path and the high interferometric stability required. This could be solved by adopting the phase retrieval method [32] or the 4-phase-shifting method with internal reference [11] for the measurement of TM. In addition, the results of glare suppression in experiment were obviously poorer than the simulated ones. The reasons may include: the inaccuracy of the TM measurement for MMF (affected by the quality of the reference beam, and the noise especially the photon shot noise during image acquisition); the insufficient effectiveness of the phase modulation through a DMD and 4f lens system (affected by the manufacture imperfection of the DMD surface and the accuracy of spatial filtering by the 4f system), the perturbation to MMF by air flow and platform vibration during numerical phase optimization and so on.

An interesting phenomenon is that our method seems to be insensitive to the size of ROI to be suppressed in experiment, which can be observed from Fig. 5 and Media1 that a suppression factor no more than 0.174 was achieved for different ROIs. Several reasons may account for that. The first is that only 30 iterations were adopted in experiment for phase optimization for both the cases of ER and HIO, at which the optimizations did not fully converge, so the differences among different ROIs are not obvious. Then, for ER, it suffers from premature convergence accompanying with the problem of “oversaturation” (see Appendix II), which means under a certain input size, it is not always the case that a larger ROI would have a worse suppression effect. Finally, the weakened performance of our method in experiment has rendered the distinction of suppression results among different ROIs less apparent. It is emphasized that the comparisons between the constraint conditions of ER and HIO reveal that the latter can achieve stronger performance of glare suppression, which also confirms an inversely proportional relationship between the ROI size (*i.e.*, number of speckles included) and the suppression effect achieved.

In summary, a TM-based phase optimization method for fast and effective glare suppression is proposed in this work under phase-only modulation. Two types of speckle-domain constraints including ER and HIO are explored for performance comparison with the state-of-the-art GA. The simulated and experimental results indicate that alternating projection with HIO constraint is superior in terms of fast convergence and effective glare suppression. A suppression factor of 0.17 was realized by HIO for a large target region containing ~625 speckles at the distal end of the MMF. Advantages of our method include the fast and generic phase computation and the effectiveness of glare suppression for a large target region. The capability of using MMF to custom-tailor a speckle field may gain special interests for applications like super-resolution imaging via random speckle illumination, or flexible speckle optical tweezer in complex environments, etc.

#### Declaration of Competing Interest

The authors declare that they have no known competing financial interests or personal relationships that could have appeared to influence the work reported in this paper.

#### CRediT authorship contribution statement

**Shengfu Cheng:** Methodology, Software, Validation, Methodology, Writing – original draft. **Tianting Zhong:** Conceptualization, Investigation, Validation, Methodology, Writing – review & editing. **Chi Man Woo:** Validation, Methodology, Writing – review & editing. **Puxiang Lai:** Supervision, Funding acquisition, Writing – review & editing.

#### Data availability

Data will be made available on request.

#### Acknowledgments

The work was supported by Hong Kong Research Grant Council (15217721, R5029-19, C7074-21GF), Hong Kong Innovation and Technology Commission (GHP/043/19SZ, GHP/044/19GD), National Natural Science Foundation of China (NSFC) (81930048, 81627805), and Guangdong Science and Technology Commission (2019A1515011374, 2019BT02×105). The authors would also like to thank the Photonics Research Institute of the Hong Kong Polytechnic University for facility support.

#### Supplementary materials

Supplementary material associated with this article can be found, in the online version, at doi:10.1016/j.optlaseng.2022.107368.

#### References

- [1] Daniel A, Liberman L, Silberberg Y. Wavefront shaping for glare reduction. *Optica* 2016;3:1104–6.
- [2] Zhou EH, Shibukawa A, Brake J, Ruan H, Yang C. Glare suppression by coherence gated negation. *Optica* 2016;3:1107–13.
- [3] Huang D, Swanson EA, Lin CP, Schuman JS, Stinson WG, Chang W, Hee MR, Flotte T, Gregory K, Puliafito CA, Fujimoto JG. Optical coherence tomography. *Science* 1991;254:1178–81.
- [4] Volpe G, Kurz L, Callegari A, Volpe G, Gigan S. Speckle optical tweezers: micromanipulation with random light fields. *Opt Express* 2014;22:18159–67.
- [5] Mudry E, Belkebir K, Girard J, Savatier J, Moal EL, Nicoletti C, Allain M, Sentenac A. Structured illumination microscopy using unknown speckle patterns. *Nat Photonics* 2012;6:312–15.
- [6] Vellekoop IM, Mosk A. Focusing coherent light through opaque strongly scattering media. *Opt Lett* 2007;32:2309–11.
- [7] Mosk AP, Lagendijk A, Leroosey G, Fink M. Controlling waves in space and time for imaging and focusing in complex media. *Nat Photonics* 2012;6:283–92.
- [8] Horstmeyer R, Ruan H, Yang C. Guidestar-assisted wavefront-shaping methods for focusing light into biological tissue. *Nat Photonics* 2015;9:563–71.
- [9] Park JH, Park J, Lee K, Park Y. Disordered Optics: exploiting Multiple Light Scattering and Wavefront Shaping for Nonconventional Optical Elements. *Adv Mater* 2020;32:e1903457.
- [10] Yu Z, Li H, Zhong T, Park JH, Cheng S, Woo CM, Zhao Q, Yao J, Zhou Y, Huang X, Pang W, Yoon H, Shen Y, Liu H, Zheng Y, Park Y, Wang LV, Lai P. Wavefront shaping: A versatile tool to conquer multiple scattering in multidisciplinary fields. *The Innovation* 2022;3(5):100292 ISSN 2666-6758. doi:10.1016/j.xinn.2022.100292. <https://www.sciencedirect.com/science/article/pii/S266667582200088>.
- [11] Popoff S, Leroosey G, Fink M, Boccaro AC, Gigan S. Controlling light through optical disordered media: transmission matrix approach. *New J Phys* 2011;13:123021.
- [12] Vellekoop IM, Mosk AP. Phase control algorithms for focusing light through turbid media. *Opt Commun* 2008;281:3071–80.
- [13] Li H, Woo CM, Zhong T, Yu Z, Luo Y, Zheng Y, Yang X, Hui H, Lai P. Adaptive optical focusing through perturbed scattering media with a dynamic mutation algorithm. *Photonics Res* 2021;9:202–12.
- [14] Woo CM, Li H, Zhao Q, Lai P. Dynamic mutation enhanced particle swarm optimization for optical wavefront shaping. *Opt Express* 2021;29:18420–6.
- [15] Zhao Q, Woo CM, Li H, Zhong T, Yu Z, Lai P. Parameter-free optimization algorithm for iterative wavefront shaping. *Opt Lett* 2021;46:2880–3.
- [16] Woo CM, Zhao Q, Zhong T, Li H, Yu Z, Lai P. Optimal efficiency of focusing diffused light through scattering media with iterative wavefront shaping. *APL Photonics* 2022;7:046109.
- [17] Lai P, Wang L, Tay JW, Wang LV. Photoacoustically guided wavefront shaping for enhanced optical focusing in scattering media. *Nat Photonics* 2015;9:126–32.
- [18] Turtaev S, Leite IT, Altwegg-Boussac T, Pagan JMP, Rochefort NL, Gizmar T. High-fidelity multimode fibre-based endoscopy for deep brain *in vivo* imaging. *Light Sci Appl* 2018;7:92.
- [19] Zhong T, Qiu Z, Wu Y, Guo J, Li H, Yu Z, Cheng S, Zhou Y, Zhu J, Tian J, Sun L, Lai P. Optically selective neuron stimulation with a wavefront shaping-empowered multimode fiber. *Adv Photonics Res* 2022;3:2100231.
- [20] Cheng S, Zhong T, Woo CM, Zhao Q, Hui H, Lai P. Long-distance pattern projection through an unfixed multimode fiber with natural evolution strategy-based wavefront shaping. *Opt Express* 2022;30:32565–76.
- [21] Luo J, Wu Z, Wu D, Liu Z, Wei X, Shen Y, Li Z. Efficient glare suppression with Hadamard-encoding-algorithm-based wavefront shaping. *Opt Lett* 2019;44:4067–70.
- [22] Zhang H, Zhang B, Liu K, Fu X, Liu Q. Large-scale, high-contrast glare suppression with low-transmittance eigenchannels of aperture-target transmission matrices. *Opt Lett* 2021;46:1498–501.

- [23] Gerchberg RW. A practical algorithm for the determination of phase from image and diffraction plane pictures. *Optik* 1972;35:237–46.
- [24] Fienup JR. Phase retrieval algorithms: a comparison. *Appl Opt* 1982;21:2758–69.
- [25] Marchesini S. Invited article: a unified evaluation of iterative projection algorithms for phase retrieval. *Rev Sci Instrum* 2007;78:011301.
- [26] Loterie D, Farahi S, Papadopoulos I, Goy A, Psaltis D, Moser C. Digital confocal microscopy through a multimode fiber. *Opt Express* 2015;23:23845–58.
- [27] Fienup JR. Reconstruction of an object from the modulus of its Fourier transform. *Opt Lett* 1978;3:27–9.
- [28] Conkey DB, Caravaca-Aguirre AM, Piestun R. High-speed scattering medium characterization with application to focusing light through turbid media. *Opt Express* 2012;20:1733–40.
- [29] Lee WH. Binary computer-generated holograms. *Appl Opt* 1979;18:3661–9.
- [30] Cuhe E, Marquet P, Depeursinge C. Spatial filtering for zero-order and twin-image elimination in digital off-axis holography. *Appl Opt* 2000;39:4070–5.
- [31] Bianchi S, Di Leonardo R. A multi-mode fiber probe for holographic micromanipulation and microscopy. *Lab Chip* 2012;12:635–9.
- [32] Dremeau A, Liutkus A, Martina D, Katz O, Schulke C, Krzakala F, Gigan S, Daudet L. Reference-less measurement of the transmission matrix of a highly scattering material using a DMD and phase retrieval techniques. *Opt Express* 2015;23:11898–911.